J Solid State Electrochem (2012) 16:1833–1839
DOI 10.1007/s10008-012-1670-2

ORIGINAL PAPER

Impedance studies on the 5-V cathode material, $LiCoPO_4$

M. Prabu · S. Selvasekarapandian · M. V. Reddy · B. V. R. Chowdari

Received: 31 August 2011 / Revised: 26 January 2012 / Accepted: 28 January 2012 / Published online: 25 February 2012

Abstract Olivine-structured $LiCoPO_4$ is synthesized by a Pechini-type polymer precursor method. The structure and the morphology of the compounds are studied by the Rietveld-refined X-ray diffraction, scanning electron microscopy, Brunauer, Emmett, and Teller surface area technique, infrared spectroscopy, and Raman spectroscopy techniques, respectively. The ionic conductivity (σ ionic), dielectric, and electric modulus properties of $LiCoPO_4$ are investigated on sintered pellets by impedance spectroscopy in the temperature range, 27–50 °C. The σ (ionic) values at 27 and 50 °C are 8.8×10^{-8} and 49×10^{-8} S cm^{-1}, respectively with an energy of activation (E_a)=0.43 eV. The electric modulus studies suggest the presence of non-Debye type of relaxation. Preliminary charge–discharge cycling data are presented.

Keywords Lithium cobalt phosphate · Impedance spectroscopy · Electrical modulus · 5-V cathode

Introduction

In recent years, much work has focused on olivine-type $LiMPO_4$ (M=Fe, Mn, Co, and Ni) compounds as positive electrode (cathode) materials for lithium-ion batteries owing to their low cost and promising electrochemical properties (for M=Fe and Mn). Studies have shown that $LiCoPO_4$ is suitable as the 5-V cathode, whereas $LiFePO_4$ and $LiMnPO_4$ are good candidates as 4-V cathodes in accordance with their redox potentials, i.e., 3.6 and 4.1 V vs. Li/Li$^+$, respectively [1–6]. One of the inherent difficulties which limit electrochemical response of these materials is their extremely low electronic conductivity. For $LiFePO_4$ at room temperature, its electronic conductivity is around 10^{-9} S cm^{-1} [7] and the electronic conductivity of $LiCoPO_4$ is even much lower than that for $LiFePO_4$ and reach only ~10^{-15} S cm^{-1} [8, 9] and equally low ionic conductivity. Indeed, measurements on single crystals of $LiFePO_4$ by Amin et al. [10] show that σ (ionic) ~1×10^{-9} S cm^{-1} at 147 °C, along the a- and b-axes, and as expected due to anisotropy, much lower value along the c-axis. Room temperature σ (ionic) values will be much lower, since the energy of activation is 0.62–0.74 eV depending on the orientation. Polycrystalline $LiFePO_4$ may show higher values by virtue of grain boundaries and slight impurities or defects. Thus, carbon coating and select doping of other metal ions are practiced to improve the cathodic performance of $LiFePO_4$ [11]. Previously we reported the preliminary conductivity studies on $LiCoPO_4$ coated with silver paint using two-probe method [12]. We can expect little Ag ions diffusion on surface and the conductivity values partially due to Ag ion; in the present paper, we reinvestigated the σ (ionic) behavior of gold-coated $LiCoPO_4$ using four-probe method. Presently we report on the synthesis, characterization, detailed impedance studies, and preliminary electrochemical cycling behavior of $LiCoPO_4$.

Experimental

$LiCoPO_4$ was prepared by the Pechini-type polymer precursor method using high-purity raw materials (Merck, 99%

M. Prabu · M. V. Reddy · B. V. R. Chowdari (✉)
Department of Physics, National University of Singapore, Singapore 117542, Singapore
e-mail: phychowd@nus.edu.sg

M. Prabu · S. Selvasekarapandian (✉)
Department of Physics, Kalasalingam University, Krishnankoil 626 126 Tamil Nadu, India
e-mail: sekarapandian@rediffmail.com

purity): 0.1 mol each of $LiNO_3$, $Co(NO_3)_2{\cdot}6H_2O$, and $NH_4H_2PO_4$ is dissolved in double distilled water. Citric acid (purity 99.5%, Merck) and polyethylene glycol (Merck) in the molar ratio of (0.2:0.2) have been added to the above salt solution for gelation with vigorous stirring. The solution was evaporated on a hot plate; the powder was recovered, ground into fine powder, and calcinated at 850 °C for 8 h in air to form a fluffy powder.

X-ray diffraction (XRD) patterns were obtained using X-ray diffractometer (Xpert, MPD unit, PANalytical) with CuK_α radiation. Lattice parameters were obtained from the XRD data by Rietveld fitting using TOPAS-R (version 2.1) software. The morphology of the powders was examined by means of scanning electron microscopy (SEM—JEOL JSM-6700F); infrared and Raman spectra were recorded by using Varian 3100 FT-IR Excalibur Series and Renishaw 2000 units, respectively, at ambient temperature. The Brunauer, Emmett, and Teller (BET) surface area was measured by a Micromeritics Tristar 3000 (USA) unit at ambient temperature. For conductivity measurements, the powder was pressed (~1.2 ton pressure) to form a pellets (~1-mm thick and 10-mm diameter). The pellets were sintered at 600 °C for 3 h in air and cooled to room temperature. One thousand-nanometer thick gold (ion blocking electrode) was coated on both sides of the pellets using JOEL-JFC-1600 Auto fine coater to achieve a controlled contact area for the ionic conductivity measurements using Kiel-type four probe, with a variable temperature controller (Ionic Systems, model: KC 2.0, Germany) for conductivity measurements. They were carried at a temperatures (27–50 °C) using impedance analyzer (Solartron SI 1260 Impedance/Gain Phase Analyzer) in the frequency range of 1 MHz to 100 mHz with Ac amplitude of 10 mV.

For electrochemical studies, the composite electrodes were fabricated with the active material ($LiCoPO_4$), super P carbon black, and binder (Kynar 2801) in the mass ratio, 70:15:15 using *N*-methyl pyrrolidinone as solvent. To study the effect of mixing and particle size, we ball milled bare $LiCoPO_4$ with 15 wt.% carbon super P carbon black for 3 h using ball miller; further details of the instrument have been described previously [13]. Electrodes with thickness of ~10 μm were prepared using an etched aluminum foil as current collector using doctor-blade technique. Lithium metal foil, 1 M $LiPF_6$ in ethylene carbonate and diethyl carbonate (1:1 *v*/*v*; Merck), and Celgard 2502 membrane were used as counter electrode, electrolyte, and separator, respectively, to assemble coin-type cells (size 2016) in Ar-filled glove box (MBraun, Germany). The active material content in the electrode was around ~4 mg. The cells were aged for 12 h before the measurement. Charge–discharge cycling has been carried out at room temperature by using a computer-controlled Bitrode multiple battery tester (Model SCN, Bitrode, USA).

Results and discussion

Structure and morphology

The prepared $LiCoPO_4$ powder is violet in color. Figure 1 shows the Rietveld-refined X-ray diffraction pattern and could be indexed and refined with an orthorhombic olivine structure (space group, Pnmb). The obtained unit cell parameter values, a=5.927(5) Å, b=10.286(3) Å, and c=4.726 (3) Å match well with the reported values (JCPDS file, 32-0552). No impurity phases are observed. Scanning electron micrographs photographs show agglomeration of submicron particles with a plate-like morphology (Fig. 2a, b). The measured BET surface area of $LiCoPO_4$ is 0.065 (±0.01) $m^2\ g^{-1}$, which is typical of well crystalline material.

Infrared and Raman studies

The FT-IR probes the structure of $LiCoPO_4$ at the molecular scale, accessing the vibration modes of the ions, primarily associated to the motion of cobalt and phosphate. The infrared (IR) spectrum of $LiCoPO_4$ in the absorbance mode in the range 400–1600 cm^{-1} is shown in Fig. 3a. The bands in the range 472–651(±3) cm^{-1} are bending modes (ν_2 and ν_4) involving $(PO_4)^{3-}$ symmetric and asymmetric modes and Li vibrations. The part of the spectrum in the range 966–1,153 (±3) cm^{-1} corresponds to the stretching modes (ν_1 and ν_3) of the $(PO_4)^{3-}$ units. They involve symmetric and asymmetric modes of the P–O bonds at frequencies closely related to those of the free molecule. Our observed that vibrational bands are in close agreement with those of Julien et al. [14]. Similar to IR bands, in Raman spectra, the bands in the region 400–1,000 cm^{-1} are characteristic of stretching and bending vibrations involving the motion of oxygen atoms inside the $(PO_4)^{3-}$ tetrahedral unit. The Raman spectrum of the $LiCoPO_4$ is shown in Fig. 3b. The very sharp band at 947(±3) cm^{-1} is attributed to the A_g mode of ν_1 (symmetric stretching mode of PO_4^{3-} anion), while the weak band

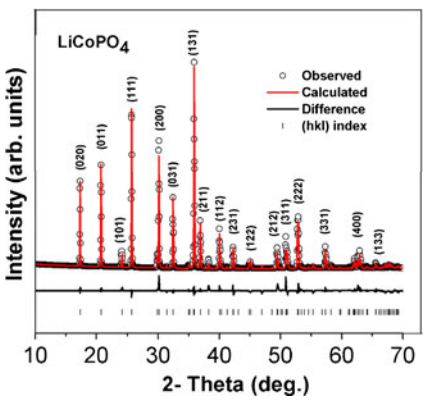

Fig. 1 Rietveld-refined X-ray diffraction pattern of $LiCoPO_4$. CuK_α radiation

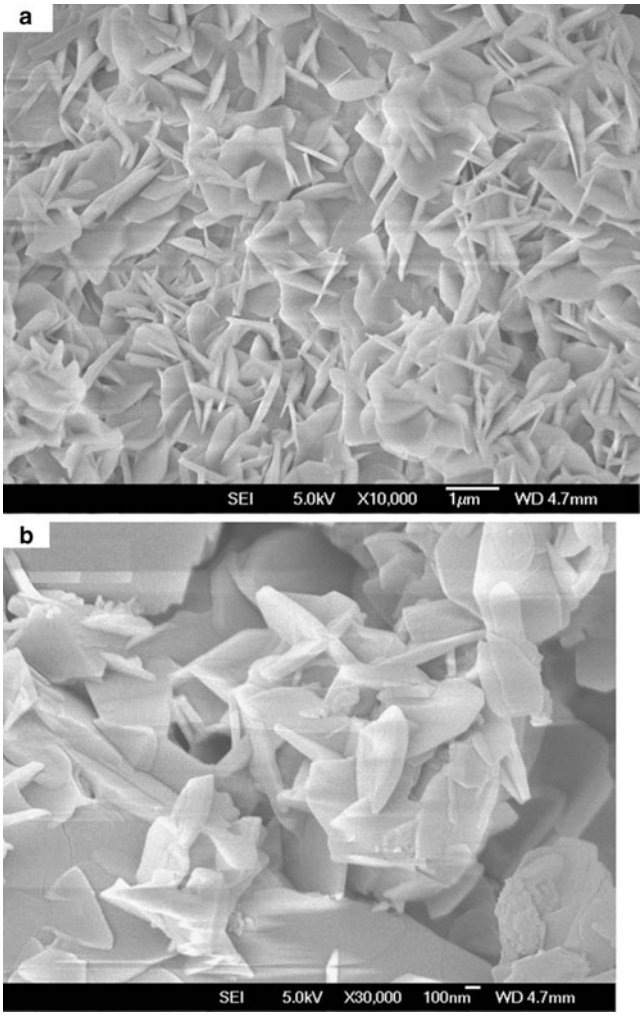

Fig. 2 SEM image of $LiCoPO_4$; **a** bar scale, 1 μm; **b** bar scale, 100 nm

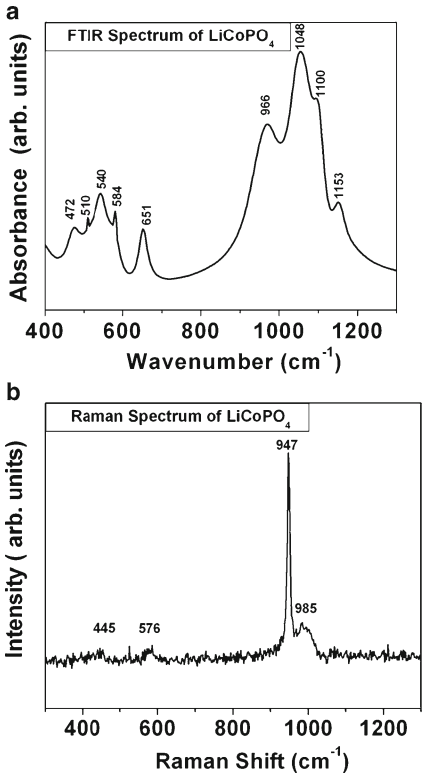

Fig. 3 **a** Infrared (IR) and **b** Raman spectrum of $LiCoPO_4$; recorded at room temperature

around 985(±3) cm^{-1} belong to the asymmetric stretching mode of the PO_4^{3-} anion (ν_3). The two weak bands observed around ~445(±3) and 576(±3) cm^{-1} comprise the bending modes of PO_4^{3-} anion [15, 16].

Impedance analysis

Impedance spectral analysis is a well-adopted technique to study the dielectric response as a function of frequency and temperature and obtain a wealth of information on ionic—and electronically—conducting solids. The electrical response of the sample is usually manifested as capacitive and resistive behaviors attributed predominantly to the bulk grains, the grain boundaries, or the defects present at the sample–electrode interface.

The Nyquist (Z' versus $-Z''$) plots for $LiCoPO_4$ in the temperature range, 27–50 °C are presented in Fig. 4a with the equivalent circuit in Fig. 4b. These Cole–Cole plots display semicircles followed by an inclined straight line at lower frequencies. As the temperature is increased, it can be seen that all the depressed semicircles (which do not touch the x-axis) shift to higher frequencies and decrease in size, resulting in a smaller intercept value with the real axis (Z'). The high-frequency and low-frequency arcs arise from bulk relaxation and interfacial effects, respectively. The high-frequency data are due to ionic migration (Li-ions in $LiCoPO_4$) through the bulk of the material which can be modeled to an equivalent electrical circuit comprising of a parallel combination of bulk resistance (R_b) and bulk capacitance (C_b) [17]. The spectra were fitted to an equivalent circuit consisting of bulk resistances (R_b) and constant phase element (CPE_{el}) in lieu of the capacitance due to non-Debye nature of the material. Bulk resistance values (R_b) are obtained from the low-frequency intercept of the semicircle on the real, (Z')-axis using the program "EQ" developed by Boukamp [18] for the analysis of impedance data. The σ (ionic) calculated using the equation:

$$\sigma(\text{ionic}) = L/R_b A \quad (1)$$

where L is the thickness and A is the geometrical area of the pellet. The σ (ionic) value of the $LiCoPO_4$ is 8.8×10^{-8} S cm^{-1} at 27 °C and increases to 49×10^{-8} S cm^{-1} at 50 °C.

Conductivity spectra analysis

The ionic conductivity (ac) of the material has been investigated in the temperature range 27–50 °C. Figure 5a shows

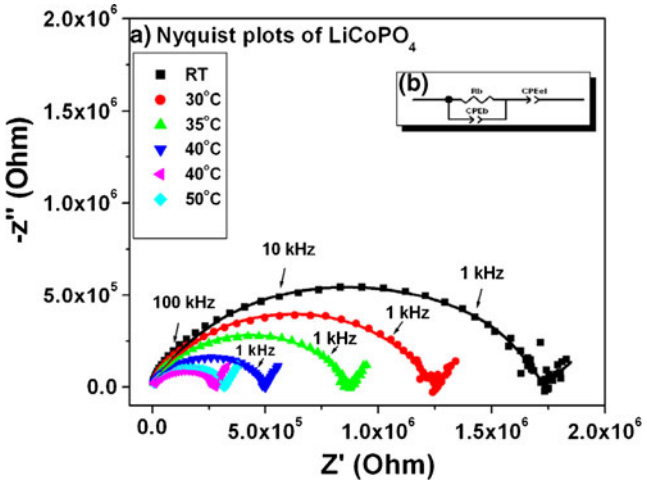

Fig. 4 **a** Complex impedance spectra (Nyquist plots) of $LiCoPO_4$ at temperatures 27–50 °C; **b** equivalent electrical circuit to fit the data. *Symbols* represent experimental data and *continuous lines* represent fitted spectra using equivalent circuit

the frequency dependence of ac conductivity, σ(ω) at various temperatures. It is evident from the figure that at low frequencies, conductivity shows frequency-independent nature of the sample which gives rise to dc conductivity

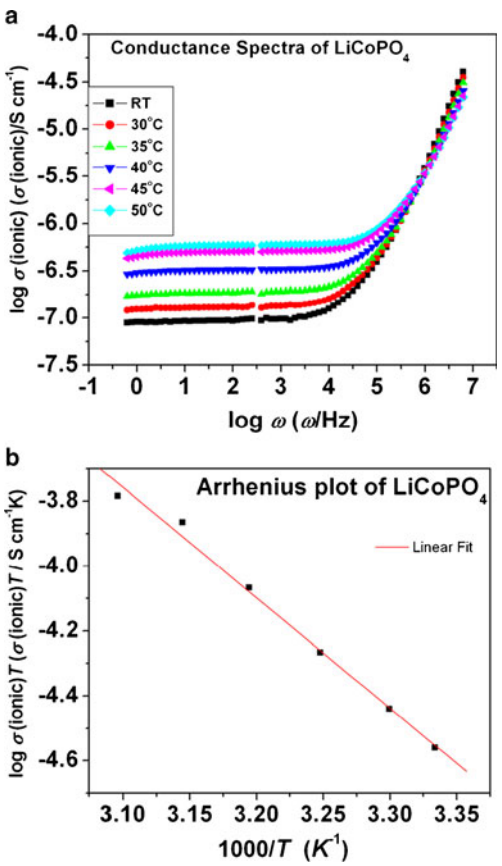

Fig. 5 **a** Conductance spectra of $LiCoPO_4$ recorded in the temperature range 27–50 °C. **b** Arrhenius plot (σT vs. $1/T$) of $LiCoPO_4$ for calculation of energy of activation, E_a

of the material. However, at the higher frequencies, σ exhibits frequency dispersion. The ac conductivity of the sample increases with the increase of temperature. At high frequencies, the conductance spectra at different temperatures converge. This indicates that the ac conductivity is independent of temperature at high frequencies. The ac conductivity, σ(ω), obeys the Jonscher's power law [19] and it is found to vary with angular frequency (ω).

$$\sigma(\omega) = \sigma(\mathrm{o}) + A\omega^n \tag{2}$$

where σ (ω) is conductivity at a particular frequency, σ(o) is dc conductivity of the sample, A is a constant and n is power law exponent and varies from zero to one ($0<n<1$).

The temperature dependence of σ (ionic) is found to obey the Arrhenius equation,

$$\sigma(\mathrm{ionic})T = \sigma_0 \exp(-E_a/kT) \tag{3}$$

where σ_0 is the preexponential factor, T is the absolute temperature (in Kelvin), k is the Boltzmann constant, and E_a is the activation energy. From Fig. 5b, the E_a=0.43 eV. In 2006, Molenda et al. [20] performed AC impedance measurements on polycrystalline $LiFePO_4$. Their results indicate that the E_a~0.63 eV (temp. range, 27–400 °C) and the σ (ionic) is same order of magnitude smaller at 27 °C (~0.9×10^{-8} S cm^{-1}). In our earlier report, we observed an E_a~0.48 eV and the σ (ionic) at 27 °C of ~1.08×10^{-8} S cm^{-1} using the two-probe technique with silver paint as blocking electrode [12].

Dielectric analysis

The dielectric properties of any system may be characterized by frequency-dependant parameters, which may define the complex permittivity (ε^*). ε' and ε'' are calculated using the impedance data by the following equation:

$$\varepsilon^* = \varepsilon' - j\varepsilon'' = 1/(j\omega C_o Z^*) \tag{4}$$

where ε' and ε'' are the real and imaginary parts of dielectric permittivity, Z^* is complex impedance, C_o the vacuum capacitance of the empty measuring cell, ω ($\omega=2\pi f$ where f is the frequency) is the angular frequency and $j=(-1)^{1/2}$. The variation of real part of dielectric constant (ε') of $LiCoPO_4$ at different temperatures as a function of ω is shown in Fig. 6. It can be seen that the ε' has a small value at room temperature where space-charge effects are negligible. At low frequencies (<1 kHz) and at higher temperatures (>35 °C) ionic migration takes place and results in an increase in ε' by creation of space-charge layers at the electrodes [21]. The value of ε' has been found to decrease with an increase in the frequency and become saturated at higher frequencies (>10 kHz). It is interesting to note that the ε' value becomes constant at relatively higher

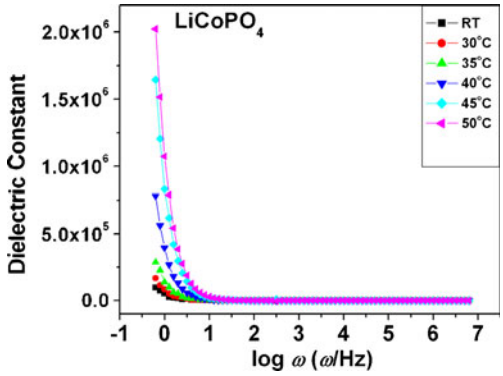

Fig. 6 Dielectric spectra of $LiCoPO_4$ at various temperatures. Dielectric constant (ε') vs. log angular frequency (ω)

frequencies when the temperature is raised. This may be due to the fact that, at high temperatures, the jump frequency of the mobile ion is large and resonates with the frequency of the applied electric field.

Complex modulus analysis

The ion transport process in ionic conductors has been studied in terms of electrical modulus spectrum. The modulus formalism in which an electric modulus M^* is

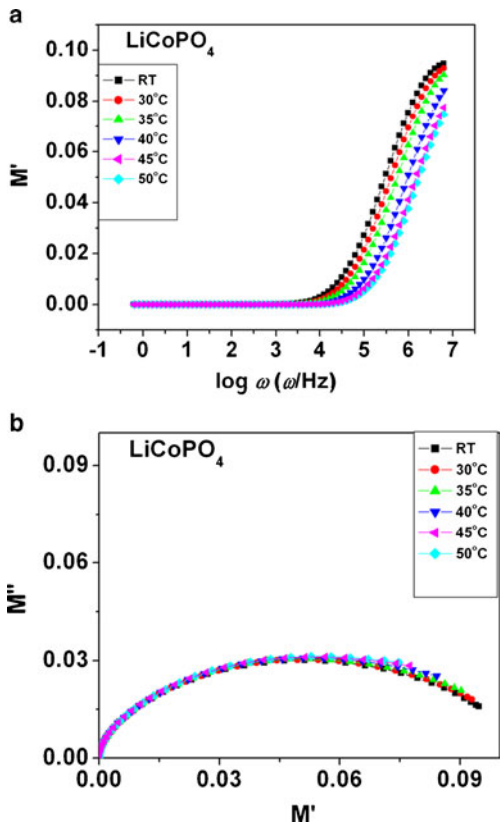

Fig. 7 Modulus spectra of $LiCoPO_4$ at various temperatures. **a** Real part of modulus (M') vs. log ω; **b** complex modulus spectra (M' vs. M'')

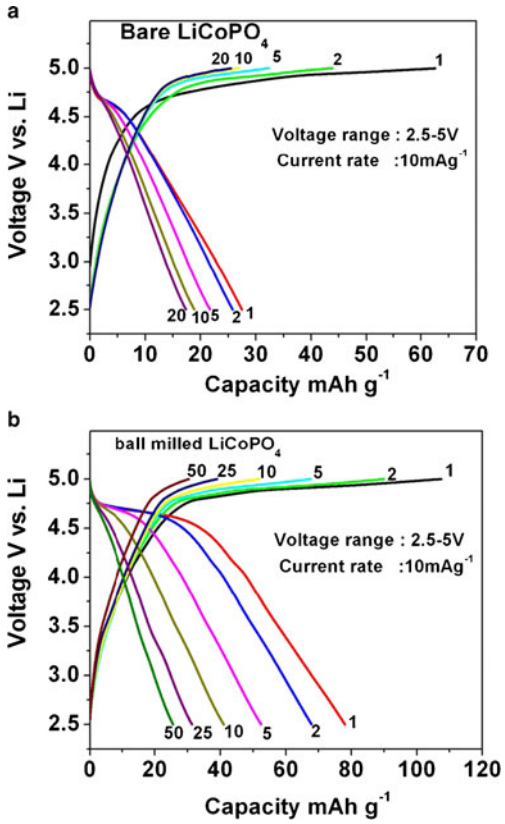

Fig. 8 Galvanostatic charge–discharge cycle curves for **a** bare $LiCoPO_4$ and **b** ball-milled $LiCoPO_4$. The numbers indicate cycle number. Current rate of 10 mA g^{-1}, potential window 2.5–5 V

defined in terms of the reciprocal of the complex relative permittivity (ε^*):

$$M^* = 1/\varepsilon^* = M' + jM'' \tag{5}$$

where M' and M'' are real and imaginary parts of modulus. The variation of real part of modulus spectrum at different temperatures for $LiCoPO_4$ is shown in Fig. 7a. It can be seen that at lower frequencies (<10 kHz), M' approaches zero indicating that the electrode polarization makes a negligible contribution

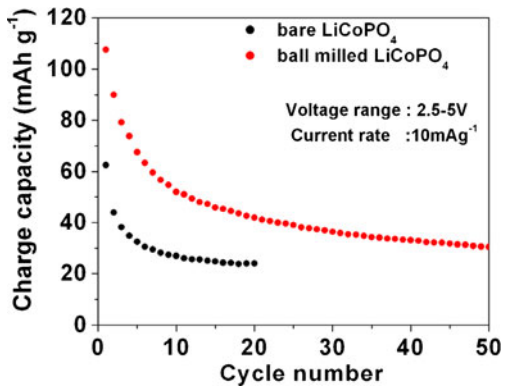

Fig. 9 Capacity vs. cycle number plots for bare $LiCoPO_4$ and ball-milled $LiCoPO_4$

to M′ and the dispersion is mainly due to conductivity relaxation [22]. The gradual variation of M' indicates that the relaxation processes are spread over a range of angular frequencies [23].

The complex modulus spectrum (M' vs. M'') of $LiCoPO_4$ is shown in Fig. 7b. The pattern is characterized by the presence of semicircular arcs at different temperatures such that they appear to be overlapping for all the temperatures. This may possibly be attributed to the presence of electrical relaxation phenomena. The semicircles with their centers lying below the real axis indicate spread of relaxation times with different time constants and hence support the non-Debye type of relaxation in the compound. It is clear that the prominent (single) semicircle is consistent with the single-phase character of the synthesized $LiCoPO_4$ [24].

Electrochemical studies

The capacity vs. voltage profiles at selected charge and discharge cycles of bare $LiCoPO_4$ at a current rate of 10 mA g^{-1} in the voltage range of 2.5–5.0 V vs. Li up to 20 cycles are shown in Fig. 8a. Surprisingly, the electrochemical extraction of Li from $LiCoPO_4$ seems to be quasi-irreversible. In all cases, voltage plateaus close to 4.9 V were observed while charging the cell, and these plateaus do not appear distinctly at the following discharge. The potential instability was detected at the charge plateau which is probably caused by the additional electrochemical process, namely, by the decomposition of electrolyte or corrosion of current collectors [25–27]. Rabanal et al. [28] and Fu et al. [6] reported that the presence of carbon additives in the grinding media which enables a good carbon coating of $LiCoPO_4$ will help in improving the reversible capacity by improving the interparticle and intraparticle electronic conductivity. In order to ascertain the influence mechanical mixing (ball milling), we studied the charge–discharge cycling of the ball-milled $LiCoPO_4$ and the plots are shown in Fig. 8b. The electrochemical performance of the ball-milled $LiCoPO_4$ was found to be better then bared one at a current rate of 10 mA g^{-1}over the voltage window 2.5–5 V. The high specific capacity is obtained when $LiCoPO_4$ is milled with carbon owing to a better interface between carbon and $LiCoPO_4$ and to the reduction of the active material particle sizes.

The charge capacity vs. cycle number plot for bare $LiCoPO_4$ is shown in Fig. 9. The charge capacity continuously decreases from 62(±3) mAh g^{-1} up to 15 cycles to 24 (±3) mAh g^{-1} and seems to stabilize thereafter, whereas ball-milled $LiCoPO_4$ showed a first charge and discharge capacity of 107(±3) and 77(±3) mAh g^{-1} and it deliver reversible capacity of 45(±3) and 30(±3) mAh g^{-1} resp. at the end of the 15th and 50th cycle (Fig. 9). The above result thus clearly demonstrates that the effects of ball milling help some extent on improved electrochemical performance. Evidently, the capacity loss in $LiCoPO_4$ has a more complicated nature for both cases. However, it has been revealed that $LiCoPO_4$ nanoparticles smaller than 100 nm exhibits better cyclic stability and clear voltage plateaus [29, 30]. But from our SEM images and BET surface area, results show that the prepared compound is in submicron range. Therefore, more efforts on exploring experimental conditions to synthesize the $LiCoPO_4$ particles with further reduced size by this method are still needed in future. Further, the different side reactions resulting from the electrolyte oxidation can deteriorate the performance of cathode material, and this is due to the thermodynamic instability of the electrolyte at the operation voltage close to 5 V vs. Li.

Conclusions

$LiCoPO_4$ has been prepared by the Pechini-type polymer precursor method and characterized by X-ray diffraction, SEM, BET surface area, and IR and Raman studies. Impedance spectral analysis shows the ionic conductivity, σ (ionic)= 8.8×10^{-8} S cm^{-1} at 27 °C and increases to 49×10^{-8} S cm^{-1} at 50 °C with the E_a=0.43 eV. The modulus analysis studies show the presence of non-Debye type of relaxation in $LiCoPO_4$. Preliminary charge–discharge cycling in the voltage range, 2.5–5.0 V vs. Li at 10 mA g^{-1}, up to 20 cycles, shows capacity loss in agreement with the literature reports due partly to the low electronic conductivity of the compound and thermodynamic instability of the electrolyte. The ball-milled sample showed that slightly enhanced electrochemical properties due to the presence of carbon additives in the grinding media enables better interface between carbon and $LiCoPO_4$ and to the reduction of the active material particle sizes that enhances the electrical conductivity of the electrode. It can be concluded that the material may have good potential for practical application if a more stable electrolyte at high voltage is developed with optimum particle size.

Acknowledgments One of the authors (M.P.) is thankful to the Dept. of Science and Technology, Govt. of India/Japan Science and Technology Agency for JRF position in the DST/JST project. M.P. also thanks the NUS for the summer Fellowship under NUS—India Research Initiative. The authors also thank Prof. G.V. Subba Rao, Dept. of Physics, NUS for helpful discussions.

References

1. Wang F, Yang J, NuLi YN, Wang JL (2011) J Power Sources 196 (10):4806–4810

2. Bakenov Z, Taniguchi I (2010) J Power Sources 195(21):7445–7451
3. Shanmukaraj D, Wang G, Murugan R, Liu H (2008) Mater Sci Eng B 149(1):93–98
4. Kumar A, Thomas R, Karan NK, Saavedra-Arias JJ, Singh MK, Majumder SB, Tomar MS, Katiyar RS (2009) J Nanotechnol Article ID 176517, 10 pages
5. Wolfenstine J, Allen J (2004) J Power Sources 136(1):150–153
6. Sun Q, Luo J-Y, Fu Z-W (2011) Electrochem Solid-State Lett 14 (10):A151–A153
7. Herle PS, Ellis B, Coombs N, Nazar LF (2004) Nat Mater 3 (3):147–152
8. Wolfenstine J, Read J, Allen JL (2007) J Power Sources 163 (2):1070–1073
9. Wolfenstine J (2006) J Power Sources 158(2):1431–1435
10. Amin R, Maier J, Balaya P, Chen DP, Lin CT (2008) Solid State Ionics 179(27–32):1683–1687
11. Ellis BL, Lee KT, Nazar LF (2010) Chem Mater 22(3):691–714
12. Prabu M, Selvasekarapandian S, Kulkarni AR, Karthikeyan S, Hirankumar G, Sanjeeviraja C (2011) Solid State Sciences 13 (9):1714–1718
13. Reddy MV, Subba Rao GV, Chowdari BVR (2011) J Mater Chem 21(27):10003
14. Salah A, Jozwiak P, Garbarczyk J, Benkhouja K, Zaghib K, Gendron F, Julien C (2005) J Power Sources 140(2):370–375
15. Markevich E, Sharabi R, Haik O, Borgel V, Salitra G, Aurbach D, Semrau G, Schmidt MA, Schall N, Stinner C (2011) J Power Sources 196(15):6433–6439
16. Julien CM, Ait Salah A, Gendron F, Morhange JF, Mauger A, Ramana CV (2006) Scripta Materialia 55(12):1179–1182
17. Maier J (2003) Solid State Ionics 157(1–4):327–334
18. Boukamp BA (1986) Solid State Ionics 18-19(Part 1):136–140
19. Jonscher AK (1977) Nature 267(5613):673–679
20. Molenda J, Ojczyk W, Swierczek K, Zajac W, Krok F, Dygas J, Liu R (2006) Solid State Ionics 177(26–32):2617–2624
21. Hodge IM, Ingram MD, West AR (1976) J Electroanal Chem Interfacial Electrochem 74(2):125–143
22. Chowdari BVR, Gopalakrishnan R (1987) Solid State Ionics 23 (3):225–233
23. Pant M, Kanchan DK, Gondaliya N (2009) Mater Chem Phys 115 (1):98–104
24. Majhi K, Varma KBR, Rao KJ (2009) J Appl Phys 106(8):084106
25. Jang IC, Lim HH, Lee SB, Karthikeyan K, Aravindan V, Kang KS, Yoon WS, Cho WI, Lee YS (2010) J Alloys Comp 497(1-2):321–324
26. Wolfenstine J, Lee U, Poese B, Allen JL (2005) J Power Sources 144(1):226–230
27. Amine K, Yasuda H, Yamachi M (2000) Electrochem Solid-State Lett 3(4):178–179
28. Rabanal ME, Gutierrez MC, Garcia-Alvarado F, Gonzalo EC, Arroyo-de Dompablo ME (2006) J Power Sources 160(1):523–528
29. Doan TNL, Taniguchi I (2011) J Power Sources 196(13):5679–5684
30. Lloris JM, Pérez Vicente C, Tirado JL (2002) Electrochem Solid-State Lett 5(10):A234